AIAA 81-0753R

Magnetoelectrostatic Thruster Physical Geometry Tests

W.D. Ramsey*
Xerox Electro-Optical Systems, Pasadena, Calif.

Inert gas tests were conducted with several magnetoelectrostatic containment (MESC) discharge chamber geometries. The configurations tested included three discharge chamber lengths; three boundary magnet patterns; two different flux density magnet materials; hemispherical- and conical-shaped thrusters with different surface-to-volume ratios; and two- and three-grid ion optics. Argon mass utilizations of 60-79% were achieved at 210-380 eV/ion in different test configurations. Short hemithruster configurations produced 70-92% xenon mass utilization at 185-220 eV/ion.

Introduction

THE work described below is a continuation of the inert gas discharge optimization effort that was begun several years ago by the author.[1] Discharge optimization is aimed at producing the maximum propellant mass utilization efficiency at minimum discharge energy consumption for use in space flight and terrestrial applications. Magnetoelectrostatic design discharge chambers were selected for optimization owing to excellent performance achieved with mercury and cesium in previous programs.[2,3] Thrusters with 12-cm diameter were used for the sake of convenience, as more MESC hardware of this size existed at the outset.

The investigation discussed in the paper concentrated on performance improvements that could be gained by changes in existing MESC geometry. Two means of performance improvements were explored. First, discharge chamber length was increased to explore the tradeoffs between increases in neutral residence time and ionic recombination losses. Second, different permanent magnet spacings and magnets were tested to determine which combination produced the best inert gas performance with the MESC geometry.

Apparatus

Platinuum-Cobalt Hemi Thuster

Two different hemispherical-shaped thrusters and a conical-shaped thruster were used in testing. The first hemi thruster was designed as a cesium discharge thruster in a previous program[3] and loaned for these inert gas tests. The cesium design hemi thruster used a low anode magnetic field that matched 20-V cesium plasma potential. Platinum-cobalt magnet rings with average fields of 0.11 T were used in the design, shown in Fig. 1.

Conversion to inert gas operation consisted of replacing the hollow cathode with the assembly shown in Fig. 2 and relocating the anodes closer to the magnets. The 3.2-mm-diameter cathode subassembly consisted of alternate tubes of boron nitride and stainless steel to electrically isolate and support the keeper and baffle disks. The baffle support tube axial position was controlled by means of a vacuum tight rod assembly.

The boundary anodes were relocated closer to the platinum-cobalt boundary magnets to increase the anode magnetic field for inert gas operation at greater plasma potential. During anode relocation the magnetic field was found to vary as much as a factor of 2 along the same anode ring. To compensate for this, anode rings were divided into four sections to permit independent radial movement of the sections and thus locate the anodes in a uniform magnetic field. The electron current to each section was monitored and the anode sections positioned for uniform current density.

Ion Optics

Performance of the Pt-Co magnet hemi thruster was mapped with two- and three-grid ion optics. The two-grid assembly consisted of two 0.25-mm-thick molybdenum grids hydroformed into a 4.0-mm-deep dish. The 2200 grid holes were set on 2.5-mm centers with no beam divergence compensation. The accel and screen grid hole diameters were 1.17 and 2.24 mm, respectively.

The three-grid system was formed by adding a ground potential screen grid (decel) downstream of the accel. Intergrid gaps of 1.0 and 1.5 mm were used between the screen-to-accel and accel-to-decel, respectively.

Samarium-Cobalt Magnet Hemi Thruster

In the second hemi thruster, the platinum-cobalt magnets were replaced with samarium-cobalt magnets. The short bar sections of Sm-Co were magnetized orthogonal to the wall.

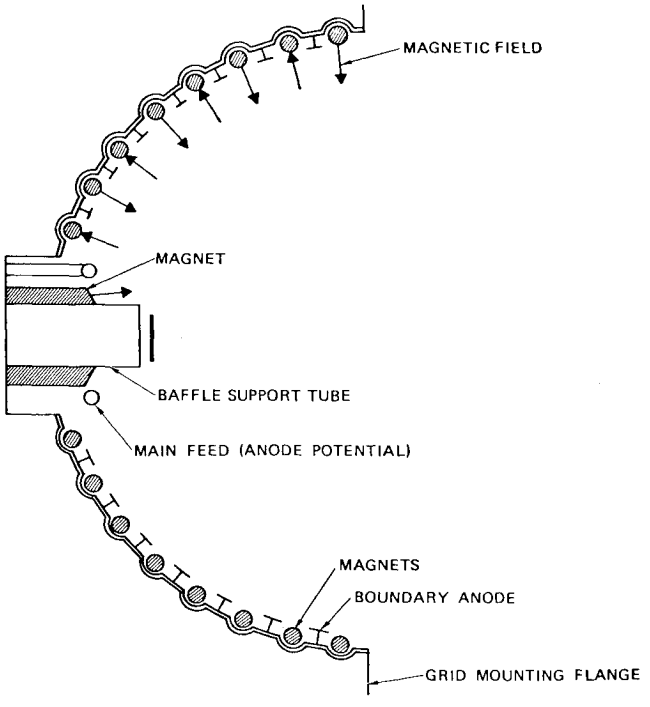

Fig. 1 Cutaway schematic of hemi thruster test assembly.

Presented as Paper 81-0753 at the AIAA/JSASS/DGLR 15th International Electric Propulsion Conference, Las Vegas, Nev., April 21-23, 1981; submitted April 29, 1981; revision received Oct. 26, 1981.

*Physicist. Member AIAA.

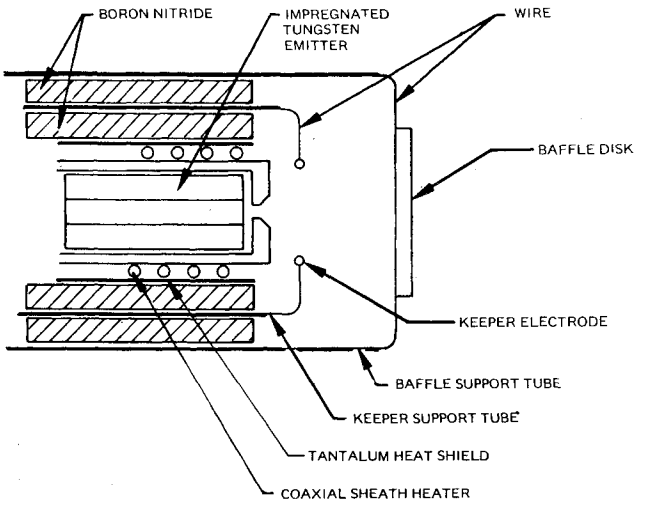

Fig. 2 Cathode subassembly.

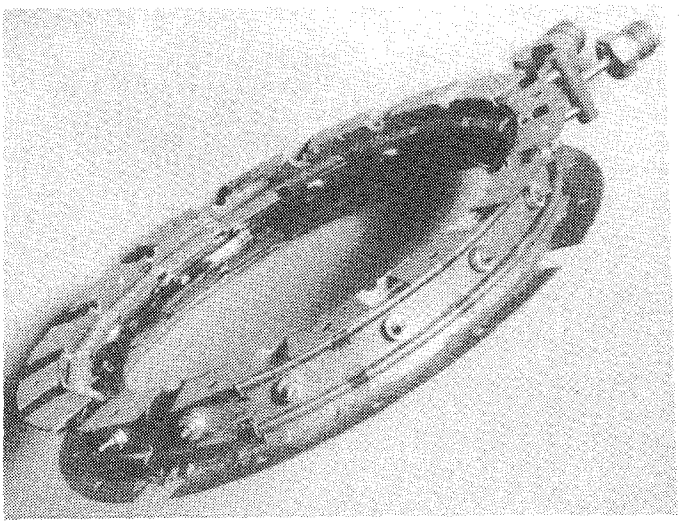

Fig. 3 Hemi thruster extension spool with samarium-cobalt magnets and cooling coils.

This magnet configuration had a uniform magnetic field which was greater than the average field of the platinum-cobalt magnets. The pole face magnetic field increased from 0.11 to 0.21 T owing to the material change.

Inert gas performance tests were conducted with 5.7-, 8.0-, and 10.3-cm-long thruster Sm-Co magnet assemblies. The longer assemblies were produced by adding 2.3-cm-long cylindrical sections to the grid mounting flange of the discharge chamber. Each section contained two Sm-Co magnet rings and two anodes. Although the anodes were divided into sections, differential section radial adjustment was not necessary to achieve uniform anode current density. A photograph of a 2.3-cm-long cylindrical section ("spool") is shown in Fig. 3.

Figure 3 shows several interesting features of Sm-Co spool thruster construction. Nitrogen gas flow through the copper cooling coils was used to keep the magnets cooler than the 250°C demagnetization temperature. The notched flange design allowed the MESC anode-magnet pattern to be maintained throughout the discharge chamber.

Conical Thruster

The 12-cm conical thruster was designed for maximum flexibility. A set of anode insulator mounting holes in the chamber walls and the smooth conical and cylindrical surfaces permitted the magnet and anode spacing to be changed from the nominal 1.2-cm center-to-center spacing to either a 1.8- or 2.3-cm spacing (pitch). A 6.4-mm hollow cathode was incorporated in the design to prevent overtemperature operation seen during 3.2-mm hollow cathode tests. The conical thruster is depicted in Fig. 4.

The conical thruster was designed as a 5.7-cm-long assembly that could be lengthened as desired. Tests were conducted with the 5.7- and 8.0-cm-long assemblies using the 1.3-cm magnet pitch. The 8.0-cm length was used to test the 1.8-cm magnet pitch. A 9.0-cm-long assembly accommodated the 2.3-cm magnet pitch.

Test Instrumentation

Thruster power conditioning and gas flow control were provided by the same units described in Ref. 1. The power conditioning consisted of dc commercial supplies and a 20-kHz inverter, while gas flow to the main plenum and cathode was controlled with needle valves and monitored with a mass flow transducer.

Beam Probe

Beam spread and beam flatness were calculated from Faraday cup probe data. Two 1.3-cm-diam Faraday cup probes were located 22 and 20 cm downstream of the grid

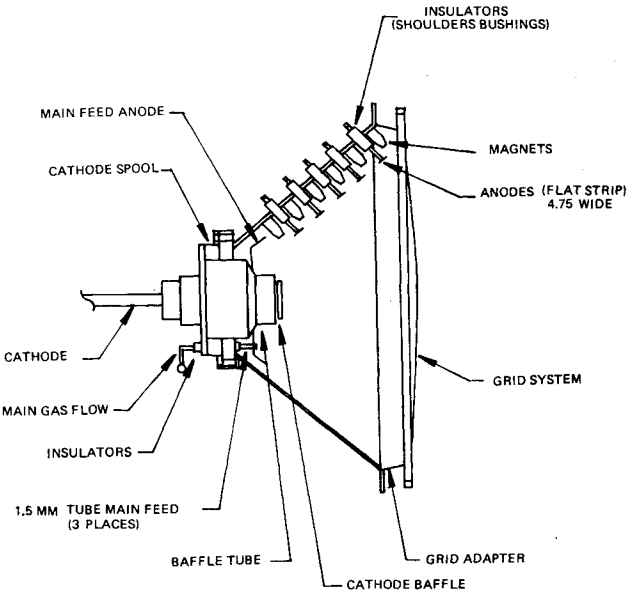

Fig. 4 Schematic of 5.7-cm-long conical thruster assembly.

system. The ion beam current seen by the cups was plotted on a ground potential *x-y* recorder.

Time-of-Flight Apparatus

The MESC thruster tests time-of-flight (TOF) data were used to determine how changes in thruster physical geometry affected the percentage of double- and single-charged ion currents in the exhaust beam. The TOF data were also used to calculate the equivalent single-charged ion beam or beam ion current. The equivalent single-charged ion beam was used for mass utilization and eV/ion calculations.

The 60-cm-diam TOF collector was located on the thruster centerline 3.0 m from the grid system. Photographs of oscilloscope traces were used to record TOF data. There were three traces on each photograph: a ground or zero level trace; a quiescent operational trace; and a trace of the interrupted beam. A schematic of the TOF apparatus is shown in Fig. 5. The high voltage interruption plunger was located in a grounded housing for safety. A transient triggered the scope and recorded the ion traverse time.

Test Results

Thruster performance tests usually followed the same general outline. The cathode and main flows were first

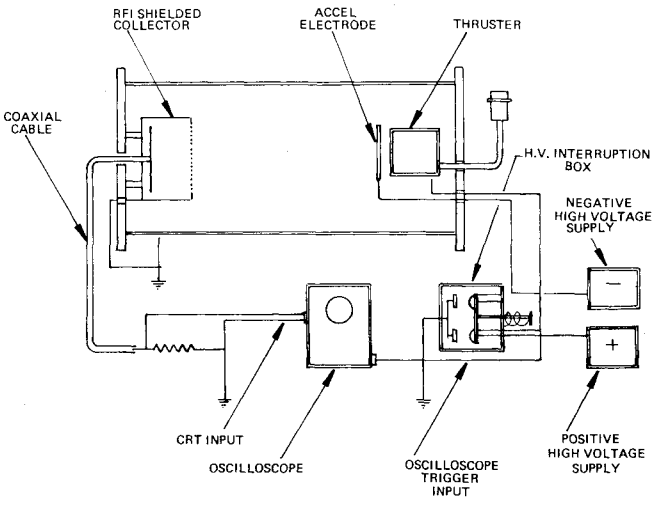

Fig. 5 Time-of-flight apparatus.

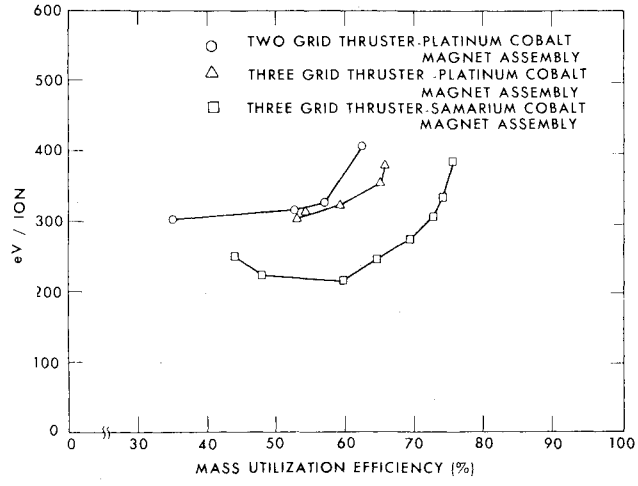

Fig. 6 Two- and three-grid ion optics argon performance comparison with 5.7-cm-long coils.

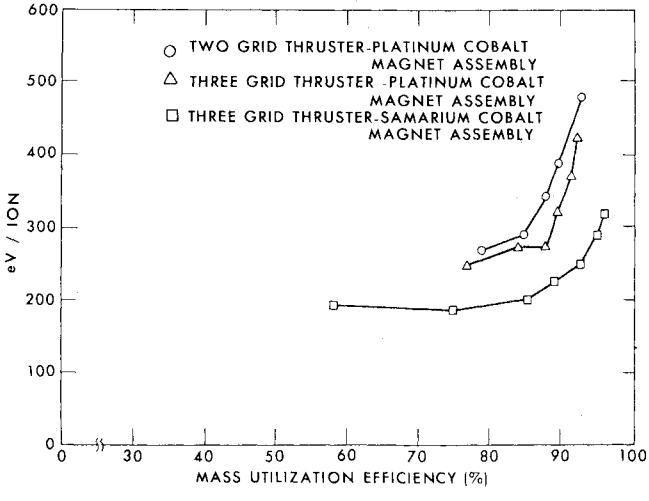

Fig. 7 Two- and three-grid ion optics xenon performance comparison with 5.7-cm-long thruster.

allowed to stabilize at selected levels. Next, the thruster configuration was performance mapped from the minimum stable anode current to a 5.0-A or greater discharge. Data were recorded after each 0.5-A change in current with the anode supply operating in the current limited mode. If the anode potential remained within 10 V of nominal and the performance curve looked promising, these data were used to characterize the total gas flow for the particular test configuration. If not, new main/cathode gas flow ratios were chosen and the data sweep repeated. Usually three or more total gas flows were tested with each thruster configuration. Typical anode potential ranged between 46 and 56 V during argon operation and 37-47 V during xenon.

Change in the baffle axial placement produced variation in apparent plasma impedance. Far downstream baffle positions, 1.3-1.5 cm from the cathode orifice, had low plasma impedance, while a close baffle location, 0.5 cm from the cathode, produced greater impedance.

Hemi Thruster Tests

Figures 6 and 7 are a comparison of the performance achieved with the different 5.7-cm-long hemi discharge chamber assemblies. Performance of the 5.7-cm Pt-Co magnet hemi thruster was optimized by locating the anode sections in a uniform 7.0-mT magnetic field. Further increases in the anode field produced a reduction in the maximum mass utilization efficiency. Moving the anodes away from the magnets to a lower magnetic field increased the discharge energy consumption.

Uniform anode magnetic fields were achieved with the Pt-Co hemi by positioning different sections of the anodes varying distance from the magnets. Anode sections were located 1.7-3.4 mm from the magnets to produce the 7.0-mT field mentioned above. Adding the third grid to the ion optics system improved thruster performance, as seen in Figs. 6 and 7. No changes were made to the discharge chamber between the two sets of tests.

The same three-grid ion optics system was used in the remainder of the MESC thruster tests. The 5.7-cm-long Sm-Co hemi thruster produced optimum performance with the anodes located 9.0 mm from the magnets in a 9.0-mT field. The anode sections were located a uniform distance from the magnets. Further increases in the anode field produced unstable discharge operation, while reduction in the field increased the eV/ion.

Figures 8 and 9 are graphs of the optimum performance of the 5.7-, 8.0-, and 10.3-cm-long Sm-Co magnet hemi thrusters. The 5.7-cm optimum performance has been repeated in these two figures for comparison.

The performance graphs show that the additional length affected operation of each propellant differently. Increasing the discharge chamber length from 5.7 to 8.0 cm improved argon performance above 74 mass utilization efficiency (η) but reduced thruster performance at lower η operation. Increasing the chamber length from 8.0 to 10.3 cm produced similar argon performance above 74% η and a further performance reduction at lower η operation.

Increasing the discharge chamber length reduced xenon performance at all operational levels. The reduction in xenon performance as the chamber length increased was partly due to a corresponding increase in the percent of double-charged ions in the beam.

Comparing results from the 5.7- and 8.0-cm-long chamber xenon tests under similar operating conditions indicated increasing chamber length increased the percentage of doubles in the beam by a factor of 1.5. Xenon test data under comparable operating conditions with the 10.3-cm chamber indicated an approximate increase in doubles by a factor of 2.5 compared to the 5.7-cm operation.

Conical Thruster Tests

Four configurations of the 12-cm conical thruster were tested with argon and xenon. Discharge chamber lengths of 5.7, 8.0, and 9.0 cm were used to test magnet spacings (pitchs) of 1.3, 1.8, and 2.3 cm. The 8.0-cm length tested 1.3- and 1.8-cm magnet pitch configurations. Figures 10 and 11 are graphs of the optimal performance achieved with each configuration during tests with argon and xenon, respectively.

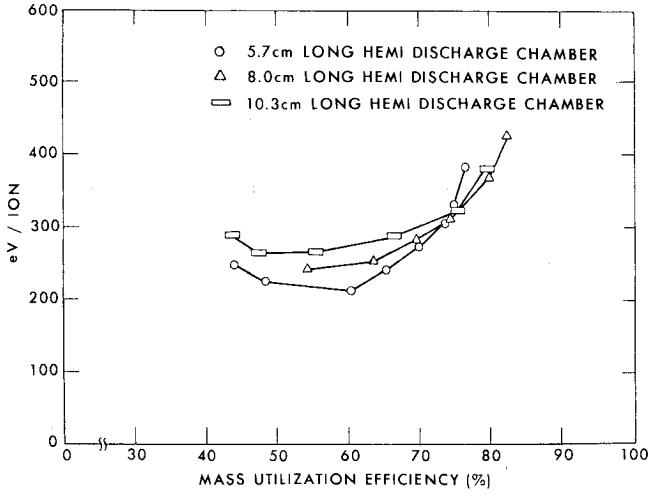

Fig. 8 Sm-Co magnet hemi thruster argon performance.

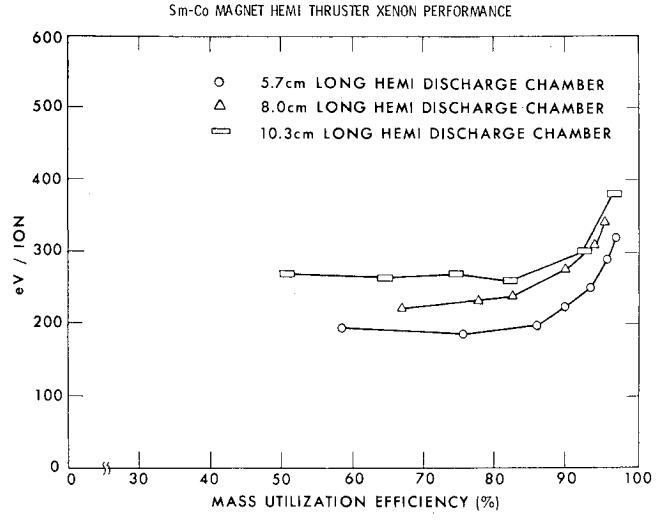

Fig. 9 Sm-Co magnet hemi thruster xenon performance.

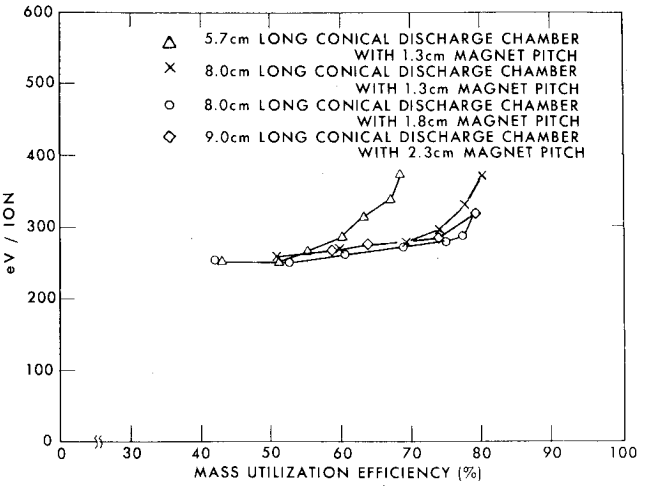

Fig. 10 Conical thruster argon performance.

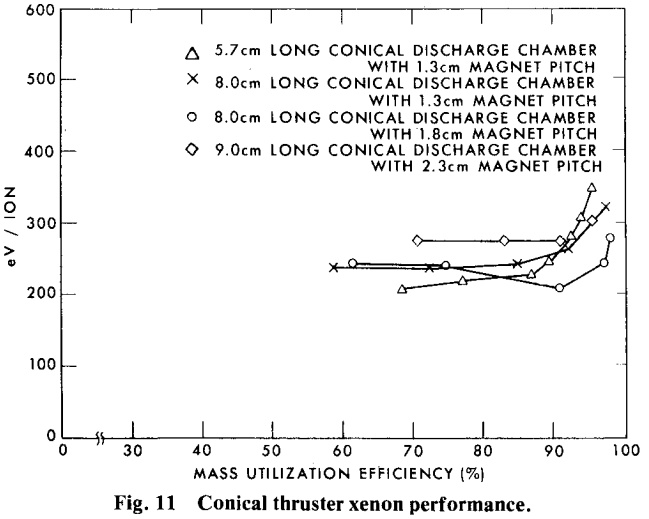

Fig. 11 Conical thruster xenon performance.

Figure 10 shows that switching from a 5.7- to 8.0-cm or longer chamber made a marked improvement in the maximum argon mass utilization obtained by the thruster. Slight differences were seen in the argon performance of the longer assemblies. For example, high mass utilization operation of the 1.8-cm-pitch magnet configuration in the 8.0-cm-long discharge was slightly better than the 1.3-cm-pitch or the 9.0-cm-long, 2.3-cm-pitch chamber.

Figure 11, xenon performance, was less clear-cut. All discharge chamber lengths and magnet pitches achieved more than 90%. Again the 8.0-cm-long chamber with 1.8-cm magnet pitch had the best mass utilization performance while the other three configurations were grouped fairly close together. The dip in the 8.0-cm-long, 1.8-cm-pitch performance curve was repeated in several sets of data.

The best conical thruster argon and xenon performance was obtained when the anode magnet fields were adjusted so they were inversely proportional to the surface area of the individual anode; i.e., small diameter anode rings were positioned in greater fields than the larger anodes. The 5.7-cm-long, 1.3-cm-pitch conical thruster displayed uniform anode current densities and produced the optimum performance shown in Fig. 10 with anode fields ranging from 8.0-14.0 mT. Similarly, the Fig. 10 performance of the 8.0-cm-long, 1.3-cm-pitch assembly had uniform anode current density and an anode magnetic field that ranged from 14.0-19.0 mT.

The anode magnetic fields in the remaining two conical thruster assemblies were calculated from the previous conical tests. Variation in the magnet pitch changed the number of anodes and anode area in the thruster. Change in anode area impacted the diffusion current density needed to achieve maximum discharge current. The anode magnetic field for the new boundary configuration was found from the inverse magnetic field Bohm diffusion relationship and the anode diameter proportionality seen in the first two conical thruster tests. For example, the 8.0-cm-long, 1.8-cm-pitch configuration had a 0.11% net reduction in anode area. The calculated magnetic field ranged from 12.6 to 17.0 mT, while the anode magnetic field producing the best results ranged from 14.0 to 17.0 mT.

The 9.0-cm-long, 2.3-cm-pitch conical assembly anode field was found to be 13.0-16.0 mT from the same calculation. Best performance was produced with variable anode widths with fields ranging from 13.5 to 16.0 mT. Use of variable widths was dictated by the asymmetric nature of the magnetic field produced by the combined conical and cylindrical chambers.

The chamber was composed of a 5.0-cm-long conical section and a 4.0-cm-long cylindrical extension. Anodes close to the junction of the two sections were found to have an edge-to-edge variation in field strength when the edges were equally spaced from adjacent magnets. The anode widths were established by locating the low field anode edge at the desired field and trimming the high field edge to match. This technique produced uniform electron current density with anode widths ranging from 0.86 to 1.1 cm.

Beam Profile Data

A summary of the beam profile data is presented in Tables 1-3. The tables illustrate the difference in two- and three-grid

Table 1 Argon beam profile with two- and three-grid systems

No. grids	Total voltage, V	Net voltage, V	I_{sp}, s	Voltage ratio	Beam half-angle, deg	Beam flatness
2	1100	900	2944	0.90	20	0.65
2	1100	600	2350	0.60	23	0.60
3	1200	900	2862	0.75	19	0.66
3	1200	700	2469	0.58	22	0.59
3	1200	500	2084	0.42	25	0.53
3	1200	300	1650	0.25	31	0.46
3	1200	200	1288	0.17	35	0.43

Table 2 Argon beam probe data with three grids

Net beam potential $V+$ Volts,	Net total potential ratio	Screen grid open area current density J_B, mA/cm^2	Beam flatness, ratio	Beam spread half-angle, deg
400	0.44	5.23	0.58	25.0
500	0.56	5.29	0.63	23.0
600	0.67	5.28	0.65	22.4
900	0.70	6.34	0.69	20.2
900	0.7	6.35	0.63	21.5
900	0.7	9.64	0.61	22.8

Table 3 Xenon beam probe data

Net beam potential $V+$ Volts,	Net total potential ratio	Screen grid open area current density J_B, mA/cm^2	Beam flatness, ratio	Beam spread half-angle, deg
400	0.33	5.7	0.75	27.6
600	0.5	5.85	0.84	23.4
800	0.67	5.98	0.92	20.1

argon operations under similar test parameters with a screen grid open area beam density of 5.7 mA/cm^2. The listed results indicate the addition of the third grid to the ion optics system reduced the minimum net potential from 600 to 200 V. Sparky operation was seen at both minimums. If the net potential was increased approximately 100 V above the minimum, operation smoothed out. The addition of the third grid had little effect on the beam flatness of the beam spread half-angle.

Tables 2 and 3 list three grid test data under different extraction potentials and beam current densities. Argon operation cited in the tables indicates increases in net potential reduced beam half-angle and increased beam flatness. Also, increases in beam density increased beam spread and reduced flatness. Similar results were seen in xenon operation. No changes in beam profile were seen in tests with the different discharge chamber lengths and magnet pitches.

Time-of-Flight Data

Time-of-flight oscilloscope traces were photographed at several discharge current levels with constant cathode-to-main flow ratios, total mass flows, and keeper current. The anode and keeper supplies were operated in a current limited mode so the respective potentials could seek the levels necessary to sustain the discharge.

The hemi thruster argon and xenon test data for a particular configuration revealed several interesting features of double-charged ion production. First, increases in anode current tend to increase the percentage of double-charged ion current in the beam. Second, to a lesser extent, double-charged current (I^{++}) increased with the potential difference between the keeper and anodes. I^{++} did not necessarily increase with anode potential alone. Third, increases in mass flow rates usually produced increases in the percentage of I^{++}.

Comparing TOF data from the different length hemi thruster tests indicates similar operational parameters produced a greater percentage of doubles in the longer chambers. Lengthening the chamber from 5.7 to 8.0 cm increases the percentage of xenon I^{++} by a factor of approximately 1.5. Increasing the chamber length from 5.7 to 10.3 cm increased xenon I^{++} by a factor of 2.5.

Examination of the 8.0-cm-long, 1.3-cm-pitch conical and 8.0-cm-long hemi-TOF data indicates similar percentages of I^{++} was present in the exhaust beams. The hemi had a discharge chamber volume surface-to-volume ratio of 0.33 cm^{-1}, and the conical thruster had a surface-to-volume ratio of 0.48 cm^{-1}. Discharge volume and surfaces were calculated using the dimension defined by the anode surfaces.

A 20-25% reduction in I^{++} was produced by increasing the magnet pitch from 1.3 to 1.8 cm in the 8.0-cm-long conical assembly. A similar reduction in I^{++} was seen in 9.0-cm-long, 2.3-cm-pitch conical assembly tests. Thus, reducing the number of anode and magnet rows in the discharge chamber assembly, reduced the percentage of on-axis I^{++} in the beam.

Conclusions

The above tests defined the geometry needed to attain the most efficient inert gas performance with the present generation design of MESC thrusters. Questions were answered as to the magnitude of the boundary magnetic field and distance between the rows of boundary magnets that produced optimum performance. Similarly, the relationship between chamber length and argon or xenon performance was

defined as well as a method of expediting the anode positioning optimization procedure.

The test results answered many of these questions but opened others. Marked performance improvements were realized by substituting 0.2 T magnets for 0.1 T magnets. The thruster performance-length relationship was found, as expected, to depend on the propellant being used. For example, the 5.7-cm-long 0.2 T magnet hemi thruster assembly achieved better performance than any previously reported, up to 88% mass utilization efficiency. Conversely, and neglecting operation less than 66% mass utilization, the best argon performance was seen with a 8.0-cm-long conical thruster with wider-than-typical MESC magnet spacing. These results are consistent with reports of other workers in the field.[4]

The percentage of multiple charged ions in the on-axis beam was found to be a function of chamber geometry and operating parameters. Tests conducted with different length thrusters indicated the percentage of double-charged ions increased with length. The length-doubles relationship was more apparent during xenon operation, where lengthening the thruster 2.3 cm increased the percentage of doubles a factor of 1.5. The percentage of doubles was also affected by the spacing of the MESC boundary magnets. Wider than typical design spacing decreased the percentage of doubles in the beam.

Changes in operating parameters during tests of the thruster configurations also affected the percentage of beam double ions. The percentage of doubles increased with anode current, total mass flow, and the potential difference between the keeper and anodes. Further investigation is needed to understand the geometry and parametric dependencies.

Acknowledgment

Work supported by NASA Lewis Research Center under Contract NAS3-21345.

References

[1]Ramsey, W.D., "Inert Gas Ion Sources," NASA CR-159423, July 1978.

[2]Ramsey, W.D., "12-cm Magneto-Electrostatic Containment Mercury Ion Thruster Development," *Journal of Spacecraft and Rockets,* Vol. 9, May 1972, pp. 318-321.

[3]James, E.L. and Ramsey, W.D., "A Prototype North-South Station Keeping Thruster," AIAA Paper 74-1119, Oct. 1974.

[4]Leung, K.N., Hershkowitz, N., and MacKenzie, K.R., "Plasma Confinement by Localized Cusps," *Physics of Fluids,* Vol. 19, July 1976, pp. 1045-1053.